

# A search for planetary nebulae in M33<sup>\*</sup>

L. Magrini<sup>1</sup>, R.L.M. Corradi<sup>2</sup>, A. Mampaso<sup>2</sup>, and M. Perinotto<sup>1</sup>

<sup>1</sup> Dipartimento di Astronomia e Scienza dello Spazio, Università di Firenze, Largo E. Fermi 5, 50125 Firenze, Italy

<sup>2</sup> Instituto de Astrofísica de Canarias, c. Vía Láctea s/n, 38200, La Laguna, Tenerife, Spain

Received 24 July 1999 / Accepted 9 November 1999

**Abstract.** We searched for planetary nebulae (PNe) in the nearby spiral galaxy M33 using the Wide Field Camera at the 2.54 m Isaac Newton Telescope of La Palma (Spain). Images in the [O III] nebular line at  $\lambda$  5007 Å, in the H $\alpha$ + [N II] lines around 6560 Å, and in the continuum around 5550 Å allowed us to detect a large number of emission line objects. Among them, 134 candidate PNe have been selected. In addition, we found 63 emission-line objects which have a non-negligible continuum emission, and for this reason they have been conservatively discarded from the group of candidate PNe. We have derived the PN luminosity function. It agrees very well with that of galaxies in the Local Group. The resulting distance to M33 is  $840 \pm 90$  kpc, in excellent agreement with the value obtained using Cepheids.

**Key words:** ISM: planetary nebulae: general – galaxies: individual: M33 – galaxies: ISM

## 1. Introduction

Extragalactic planetary nebulae (PNe) are known in almost all galaxies of the Local Group. Most of them were discovered in the last decade by means of continuum-subtracted images in the bright nebular line of [O III] at 5007 Å (Ciardullo et al. 1989; Jacoby 1989). M33, one of the two other large spiral galaxies of the Local Group besides the Milky Way, is to our knowledge the only major nearby galaxy which has not been searched for PNe yet. We aimed to fill up this gap taking advantage of new observational capabilities offered by a wide field camera which has recently become operational at the Isaac Newton telescope of La Palma. [O III], H $\alpha$  and continuum images, following the procedure described in Jacoby (1989), allowed us to detect 134 candidate PNe in M33 and a large number of other emission line objects (mostly HII regions). In this paper we report on the discovery of these PNe, describe the selection criteria and the properties of these objects. Future work is planned to study spectroscopically the individual candidates, confirm their nature

*Send offprint requests to:* M. Perinotto (mariop@arcetri.astro.it)

<sup>\*</sup> Based on observations obtained at the 2.5m INT telescope operated on the island of La Palma by the Isaac Newton Group in the Spanish Observatorio del Roque de Los Muchachos of the Instituto de Astrofísica de Canarias.

and determine their physical properties. In Sect. 2 we present the observation and data reduction. Sect. 3 contains the analysis of data. The classification of the detected emission line objects according to their size and line ratios is done in Sect. 4. With the candidates PNe we construct their luminosity function and determine the distance of M33 (Sect. 4). Conclusions are given in Sect. 5.

## 2. Observations and data reduction

All images were taken in a single night (November 11, 1998) using the Wide Field Camera (WFC) at the prime focus of the 2.54 m Isaac Newton Telescope (INT) of the Observatorio del Roque de los Muchachos in the island of La Palma (Spain). The seeing was  $1''.5$  in the first half of the night and  $2''$  in the second one. The WFC has a panoramic detector consisting of four EEV CCD  $2048 \times 4096$  pixels each, i.e. a total of  $33.55 \times 10^6$  pixels. The pixel size projects to  $0''.33$  in the sky. The whole CCD array covers a field of view of about  $34' \times 34'$ , while an additional CCD  $2048 \times 2048$  is used for guiding. The arrangement of the four rectangular CCDs makes the geometry of the field of view as shown in Fig. 1. The emission-line filters used have the following central wavelengths and full widths at half maximum (FWHM): 5008/100 Å ([O III]) and 6568/95 Å (H $\alpha$ + [N II]). We also used a Strömgren Y filter as a continuum filter, centred at 5550 Å and covering a spectral region where there are no strong nebular emission lines. Almost the whole galaxy was observed by centering the CCD array in two different positions (designated with A and B) in such a way as to have at each position also a galaxy-free region to be used for sky subtraction. At each telescope position and for each filter, we obtained three images with successive offsets of  $25''$  in order to fill the gaps between the CCDs and remove CCD defects. The approximate centre of each telescope positioning and the exposure times are given in Table 1. The night was photometric and we obtained several exposures of the emission-line standard PN PNG 205.8-26.7 (Dopita & Hua 1997).

The data were bias subtracted and flat-fielded in a standard way using IRAF. All images were aligned to a reference image, correcting for geometrical distortion. Images in the same filter were then averaged so that bad pixels and cosmic rays were

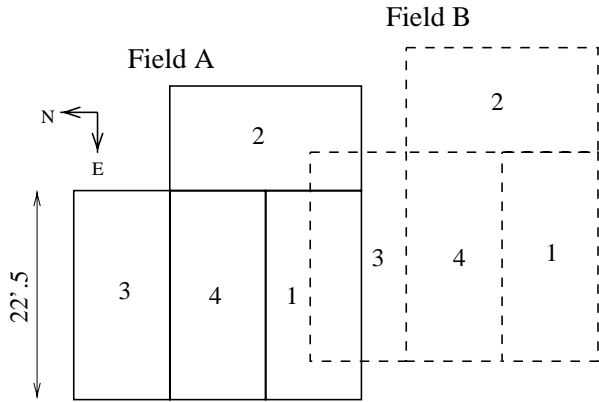


**Fig. 1.** The geometrical configuration of the 4 CCDs in the WFC and the relative position of the two telescope pointings (fields A and B) used in the present observations.

**Table 1.** Log of the observations.

Object	R.A. (2000.0)	DEC	Exp. (sec)	Filter
M33 A	01 34 00	30 53 00	300×3	H $\alpha$
M33 A	01 34 00	30 53 00	300×3	[O III]
M33 A	01 34 00	30 53 00	200×3	Ström. Y
M33 B	01 33 37	30 24 00	300×3	H $\alpha$
M33 B	01 33 37	30 24 00	300×3	[O III]
M33 B	01 33 37	30 24 00	200×3	Ström. Y

removed. Sky background, parameterized by a constant, was subtracted. We present in Fig. 2 our [O III] image of M33.

### 3. Data analysis

[O III] and H $\alpha$ + [N II] emission-line objects were selected in our images in the following way. We first computed the scale factors to be multiplied to the continuum images in order to subtract the stellar background of M33 from the [O III] and H $\alpha$ + [N II] frames. That was done by dividing the fluxes in the continuum of a large number of stars of M33 by those in the emission-line filters. The stars were automatically selected using DAOPHOT. The scaled continuum image was then subtracted from the [O III] and H $\alpha$ + [N II] images. The scale factor resulted to be around 0.7 for the correction of the continuum to both the [O III] and H $\alpha$ + [N II] frames. This procedure removed the stellar background and isolated emission-line objects, essentially HII regions and PNe. Note that the continuum filter we used has a central wavelength which is relatively far from that of the emission-line filters (especially for the H $\alpha$ + [N II] one). As a consequence, a small fraction of stars, with spectral energy distributions significantly different from “typical” stars of M33 used to compute the scale factors, are not perfectly subtracted. However, since they usually appear as “holes” either in the [O III] or H $\alpha$ + [N II] subtracted image, they can be easily distinguished from genuine emission-line objects.

The typical size of a galactic PN is of some tenths of a parsec (cf. Peimbert 1990), while evolved PNe have been found with sizes of up to 4 pc (e.g. Corradi et al. 1997). At the distance of

M33 (840 kpc, Freedman et al. 1991), 1'' corresponds to 4 pc and therefore we do not expect to resolve any PN.

For this reason, any extended emission region in our images was considered to be an HII region or a SN remnant. Candidate PNe were consequently selected among emission-line objects which are not spatially resolved. We found 197 objects of this kind, i.e. which have positive emission in the [O III] and/or in the H $\alpha$ + [N II] subtracted images, and with a spatial FWHM within  $3\sigma$  of the mean value computed using many field stars. Among them, 63 sources have a non-negligible continuum emission, i.e. the signal in the continuum filter at the position of the object is enhanced compared to its surroundings. Negligible continuum is expected from a PN, unless the central star is very luminous or has a bright companion or a foreground/background star of M33 projects at the same position as the PN. Conservatively we have excluded these 63 objects and considered as bona fide candidate PNe the remaining 134 objects listed in Table 2.

[O III] and H $\alpha$ + [N II] line fluxes were measured using AP-PHOT in the subtracted images, with photometric apertures three times the FWHMs. Errors in the fluxes were estimated considering both photometric errors, given by Poissonian statistic on background and source photons and by the detector noise, and the scattering between fluxes of the same objects measured in two different images. Photometric errors vary between few percents for the brightest objects to about 20% for the fainter ones, while systematic errors are of about 5% for [O III] and about 15% for H $\alpha$ + [N II].

An astrometric solution was computed for each frame, using the positions of bright stars in M33 given in the National Geographic Society-Palomar Observatory Sky survey. The accuracy of the coordinates of the 134 candidate PNe, which are listed in Table 2, is of about 1''. Their location within M33 is indicated by +’s in Fig. 2.

In Table 3, we list the 63 compact emission-line objects with non-negligible continuum, together with their measured [O III] and H $\alpha$ + [N II] fluxes. Since no absolute calibration for the Strömgren Y filter was available, the contribution of the continuum relative to [O III] was estimated by measuring the intensities of sources in the scaled Strömgren Y frames. With the present data, it is difficult to say whether these emission-line objects are compact HII regions, Be stars, symbiotic stars, Wolf-Rayet stars, LBVs, etc. Further spectroscopic studies are needed to clarify their nature.

## 4. Discussion

### 4.1. Contamination with compact HII regions

At the distance of M33, low-excitation PNe can be misidentified with compact HII regions.

We used the  $R=I([\text{O III}])/I(\text{H}\alpha+[\text{N II}])$  line ratio to estimate the possible contamination of HII regions in our sample of candidate PNe. The distribution of  $R$  for the 127 objects in Table 2 in which both the [O III] and H $\alpha$ + [N II] fluxes have been measured is shown in the upper box of Fig. 3. In the lower box, we show for comparison the distribution of 808 Galactic PNe whose fluxes are quoted in the Strasbourg-ESO Catalogue of Galactic

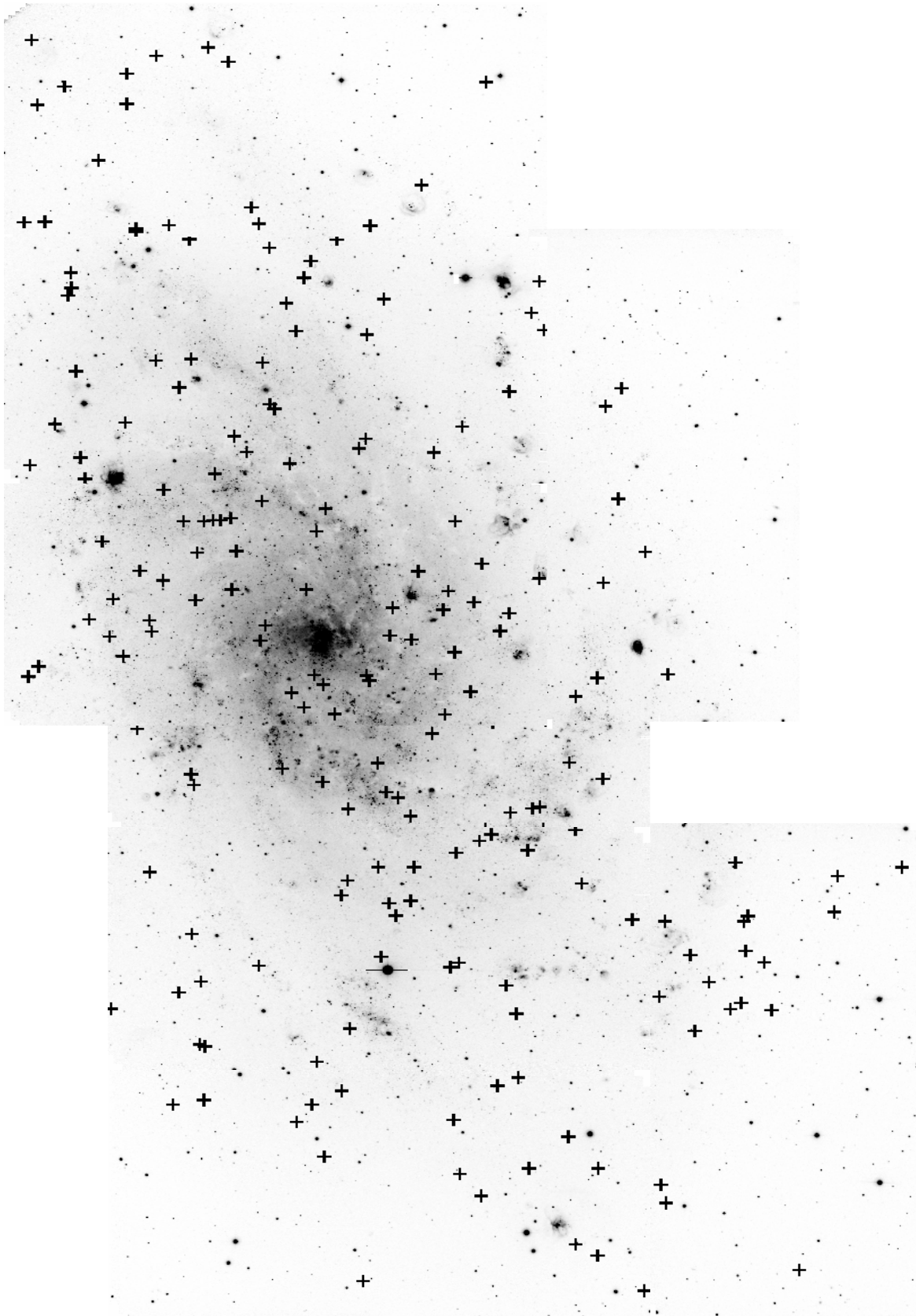


**Fig. 2.** The [O III] image of M33 obtained at the INT telescope with the Wide Field Camera. North is at the top, East to the left. The “+” symbols indicate the location of the candidate PNe. Small horizontal bars are artefacts.

**Table 2.** PN candidates found in M33. Fluxes in  $H\alpha + [N\ II]$  and in  $[O\ III]$  are in units of  $10^{-15}$  erg cm $^{-2}$  s $^{-1}$ .  $[O\ III]$  magnitudes and their adopted, individual errors, are indicated in the last two columns.

id	R.A. (2000.0)	Dec.	$F_{[H\alpha]}$	$F_{[O\ III]}$	$m_{[O\ III]}$	err	id	R.A. (2000.0)	Dec.	$F_{[H\alpha]}$	$F_{[O\ III]}$	$m_{[O\ III]}$	err
1	1 32 26.2	30 25 43	–	0.7	24.15	0.20	57	1 33 43.2	30 59 40	1.9	0.9	23.87	0.21
2	1 32 37.5	30 23 49	4.2	5.9	21.83	0.07	58	1 33 43.6	30 49 0	1.5	2.2	22.90	0.10
3	1 32 39.6	30 37 41	2.4	4.1	22.23	0.08	59	1 33 44.1	30 20 26	3.3	10.2	21.24	0.07
4	1 32 42.7	30 12 38	1.1	2.8	22.64	0.09	60	1 33 46.1	30 26 56	1.4	3.4	22.43	0.09
5	1 32 43.7	30 21 53	9.1	6.3	21.76	0.08	61	1 33 46.7	30 17 32	2.8	10.1	21.25	0.06
6	1 32 44.2	30 43 23	0.3	0.7	24.15	0.20	62	1 33 49.1	30 35 46	1.6	6.5	21.73	0.08
7	1 32 49.1	30 51 6	2.2	7.7	21.54	0.08	63	1 33 50.2	30 14 21	2.9	9.2	21.35	0.07
8	1 32 49.2	30 25 51	11.4	10.1	21.25	0.06	64	1 33 50.6	30 18 45	1.7	0.3	25.07	0.42
9	1 32 52.9	30 41 54	1.0	3.0	22.57	0.09	65	1 33 50.8	30 32 4	10.1	5.6	21.89	0.09
10	1 32 53.9	30 37 31	3.2	–	–	–	66	1 33 51.1	30 37 11	13.2	1.2	23.56	0.17
11	1 32 56.2	30 13 57	1.5	3.4	22.43	0.09	67	1 33 52.6	30 16 53	4.3	10.1	21.25	0.06
12	1 32 56.6	30 32 26	2.0	0.5	24.51	0.30	68	1 33 53.1	30 37 36	11.3	12.8	20.99	0.06
13	1 32 57.2	30 9 44	2.9	8.6	21.42	0.07	69	1 33 55.0	30 36 3	7.8	6.2	21.78	0.08
14	1 32 59.5	30 27 35	0.2	3.8	22.31	0.09	70	1 33 55.1	30 37 42	17.3	0.8	24.00	0.31
15	1 33 1.3	30 10 15	2.8	2.4	22.81	0.10	71	1 33 55.6	30 16 1	1.0	0.7	24.15	0.21
16	1 33 1.9	30 15 28	1.0	1.0	23.76	0.16	72	1 33 57.0	30 54 8	3.3	9.6	21.30	0.06
17	1 33 7.6	30 54 21	3.1	10.4	21.22	0.06	73	1 33 57.9	30 36 45	4.4	4.5	22.13	0.08
18	1 33 9.1	30 31 6	3.0	14.2	20.88	0.06	74	1 33 60.0	30 40 28	–	7.1	21.63	0.08
19	1 33 9.8	30 13 53	1.1	0.9	23.87	0.21	75	1 34 1.4	30 50 22	4.4	12.5	21.02	0.06
20	1 33 10.2	30 29 11	5.8	0.6	24.31	0.29	76	1 34 2.3	30 50 36	0.6	1.6	23.25	0.12
21	1 33 11.0	30 21 15	1.7	0.5	24.51	0.28	77	1 34 2.7	30 23 26	–	0.8	24.00	0.18
22	1 33 14.7	30 40 37	1.4	6.1	21.80	0.07	78	1 34 2.7	30 58 7	27.6	10.1	21.25	0.06
23	1 33 13.3	30 22 38	14.2	3.3	22.46	0.09	79	1 34 3.6	30 39 14	5.4	7.8	21.53	0.08
24	1 33 14.9	30 30 48	1.8	2.7	22.68	0.10	80	1 34 3.7	30 52 35	1.2	3.0	22.57	0.13
25	1 33 15.6	30 17 51	0.4	0.4	24.75	0.41	81	1 34 6.7	31 0 29	–	1.0	23.76	0.21
26	1 33 17.4	30 29 58	2.0	1.8	23.12	0.12	82	1 34 6.9	30 39 12	4.2	8.6	21.42	0.07
27	1 33 19.4	30 12 31	0.7	1.6	23.25	0.15	83	1 34 7.2	30 48 17	7.4	4.3	22.18	0.08
28	1 33 19.6	30 29 39	2.9	13.9	20.90	0.06	84	1 34 7.5	30 39 56	8.2	3.7	22.34	0.10
29	1 33 20.0	30 30 1	6.4	2.8	22.64	0.13	85	1 34 9.6	30 49 1	2.7	1.6	23.25	0.15
30	1 33 20.7	31 6 44	0.7	2.4	22.81	0.10	86	1 34 9.7	31 7 42	2.9	2.1	22.95	0.10
31	1 33 21.7	30 41 9	3.5	5.6	21.89	0.09	87	1 34 12.2	30 39 9	17.8	0.2	25.51	0.99
32	1 33 21.9	30 36 56	1.2	1.4	23.39	0.15	88	1 34 12.6	30 44 25	1.5	1.1	23.66	0.15
33	1 33 23.5	30 13 34	1.1	2.9	22.60	0.11	89	1 34 13.2	31 8 25	2.2	5.7	21.87	0.09
34	1 33 24.2	30 38 47	1.2	1.5	23.32	0.14	90	1 34 13.6	30 47 11	2.8	1.9	23.06	0.11
35	1 33 24.4	30 42 55	3.6	3.3	22.46	0.09	91	1 34 13.8	30 22 36	4.9	16.3	20.73	0.06
36	1 33 24.5	30 16 11	0.9	1.3	23.48	0.16	92	1 34 14.2	30 17 7	2.4	3.4	22.43	0.09
37	1 33 28.0	30 40 47	4.7	2.1	22.95	0.10	93	1 34 15.5	30 24 55	3.1	7.4	21.59	0.07
38	1 33 28.0	30 35 53	2.1	1.6	23.25	0.12	94	1 34 15.6	30 31 46	3.1	8.8	21.40	0.07
39	1 33 28.0	30 37 46	0.6	4.2	22.20	0.09	95	1 34 16.1	30 45 30	5.5	9.1	21.36	0.07
40	1 33 29.0	30 34 26	1.7	4.2	22.20	0.09	96	1 34 16.2	30 32 17	3.1	11.9	21.07	0.06
41	1 33 29.2	30 41 38	0.7	1.7	23.18	0.19	97	1 34 18.5	30 58 27	1.5	4.7	22.08	0.08
42	1 33 32.2	30 28 20	4.7	12.7	21.00	0.06	98	1 34 20.2	30 51 20	2.8	1.1	23.66	0.15
43	1 33 32.7	30 26 42	3.0	3.2	22.50	0.09	99	1 34 20.4	30 16 53	0.9	1.8	23.12	0.12
44	1 33 33.9	30 39 21	4.0	0.7	24.15	0.21	100	1 34 22.9	30 59 29	0.4	0.6	24.31	0.29
45	1 33 34.3	30 30 32	3.5	3.2	22.50	0.09	101	1 34 23.3	30 27 56	4.1	11.4	21.12	0.06
46	1 33 36.9	30 26 33	4.0	9.2	21.35	0.06	102	1 34 23.3	31 7 57	1.0	0.6	24.31	0.29
47	1 33 38.3	30 44 52	2.3	0.3	25.07	0.56	103	1 34 25.2	30 39 40	3.9	2.8	22.64	0.13
48	1 33 38.6	30 31 39	6.0	1.7	23.18	0.19	104	1 34 25.7	30 40 12	4.8	7.7	21.54	0.07
49	1 33 38.9	30 42 32	2.4	5.1	21.99	0.09	105	1 34 27.6	30 41 6	–	4.5	22.13	0.09
50	1 33 39.6	30 55 43	0.9	0.8	24.00	0.21	106	1 34 28.3	30 43 29	1.8	0.9	23.87	0.16
51	1 33 39.9	30 32 60	0.7	3.5	22.40	0.08	107	1 34 29.5	31 7 2	0.8	3.5	22.40	0.09
52	1 33 40.5	30 40 50	–	0.6	24.31	0.29	108	1 34 30.3	31 5 31	2.5	3.2	22.50	0.11
53	1 33 41.7	30 37 26	11.1	1.2	23.56	0.16	109	1 34 30.6	30 38 27	3.6	4.2	22.20	0.10
54	1 33 42.5	30 37 37	2.5	7.0	21.65	0.08	110	1 34 32.1	30 39 34	2.8	2.7	22.68	0.11
55	1 33 42.9	30 8 18	5.5	–	–	–	111	1 34 34.4	30 40 6	4.5	8.6	21.42	0.07
56	1 33 42.9	30 54 0	1.3	3.5	22.40	0.08	112	1 34 34.6	30 38 20	2.7	3.5	22.40	0.08

**Table 2.** (continued)

id	R.A. (2000.0) Dec.	$F_{[\text{H}\alpha]}$	$F_{[\text{O III}]}$	$m_{[\text{O III}]}$	err
113	1 34 35.4 30 45 52	2.3	1.1	23.66	0.15
114	1 34 37.7 30 43 23	1.7	2.4	22.81	0.10
115	1 34 38.6 30 45 3	0.6	0.3	25.07	0.56
116	1 34 39.3 30 42 2	1.7	–	–	–
117	1 34 40.6 30 52 3	3.9	1.8	23.12	0.16
118	1 34 40.6 30 39 17	1.2	4.9	22.03	0.08
119	1 34 40.7 30 44 56	1.6	8.4	21.45	0.07
120	1 34 41.7 31 6 20	2.8	2.8	22.64	0.13
121	1 34 42.0 30 56 46	1.4	3.2	22.50	0.09
122	1 34 42.7 30 44 57	6.5	10.7	21.19	0.06
123	1 34 44.7 30 44 53	3.4	3.1	22.53	0.09
124	1 34 44.9 30 49 29	6.9	3.9	22.28	0.10
125	1 34 47.1 30 41 6	7.5	8.2	21.48	0.07
126	1 34 47.4 30 42 29	1.9	3.3	22.46	0.09
127	1 34 47.4 30 59 28	14.4	2.8	22.64	0.13
128	1 34 47.6 31 5 21	4.2	12.4	21.03	0.06
129	1 34 48.4 30 40 6	0.7	0.6	24.31	0.29
130	1 34 50.2 30 44 52	10.0	9.3	21.34	0.07
131	1 34 51.5 30 59 25	2.9	0.2	25.51	0.95
132	1 34 51.8 30 37 15	7.5	3.4	22.43	0.09
133	1 35 5.2 30 43 55	4.7	0.9	23.87	0.21
134	1 35 6.2 30 46 25	6.9	6.4	21.74	0.08

PNe (Acker et al. 1992). The two distributions are very similar for  $R > 1$ , as expected since HII regions have generally a lower excitation class than PNe. In the sample of M33 there is an excess of objects with  $R < 1$  as compared to the Galaxy, indicating possible contamination by compact HII regions. Since the percentage fraction of PNe with  $R < 1$  in the Galaxy is 25% while it raises to 35% in the sample of M33, assuming that the distributions of  $R$  are the same in the Galaxy and in M33, we expect that around 15 objects in Table 2 could be in fact HII regions.

#### 4.2. The luminosity function (PNLF)

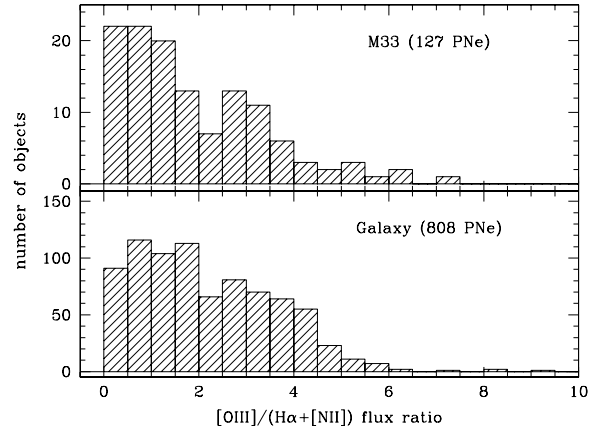
In recent years it has been shown that the PNLF is a good extragalactic secondary distance indicator (Jacoby 1997).

In order to build the PNLF, we have converted  $[\text{O III}]$  fluxes into equivalent V-band magnitudes following Jacoby (1989):

$$m_{[\text{O III}]} = -2.5 \log F_{[\text{O III}]} - 13.74. \quad (1)$$

We have then estimated the completeness of our sample for the 131 candidate PNe with measured  $[\text{O III}]$  fluxes. We calculate the signal to noise ratio (S/N) for our candidates. Ciardullo et al. (1987) found a linear relationship between S/N and completeness, putting the limit of completeness at  $S/N \sim 10$ . This would correspond in our frames to a limiting  $[\text{O III}]$  magnitude of about 23.

We note a lack of PNe in the central zone and in the densest regions along the spiral arms. This is likely due to the high stellar background in the inner disc/bulge and to the presence of many giant HII regions in the spiral arms, which make difficult to detect PNe. Another effect causing incompleteness is the galac-

**Fig. 3.** Histograms of the  $R$  for PNe in M33 and in the Galaxy.

tic background emission and the presence of large complexes of HII regions. Faint PNe can be missed because of the bright background of the inner disc, bulge and spiral arms of M33. The bulge of M33 is small, having a characteristic de Vaucouleurs' radius  $r_e$  (defined as the radius within which half the total light is emitted) of 110 arcsec (Baggett et al. 1998). Even at much shorter distances from the centre, however, the light from the disc of M33 dominates the galaxy background emission, with its tight spiral-arm design highly populated by HII regions. To avoid this high background and crowded region, we rejected from the study of the PNLF the 6 candidate PNe closer than 180 arcsec from the centre of M33. We also conservatively lowered the limiting magnitude to 22.6 mag, slightly more luminous than the point at which our observational PNLF turns down indicating incompleteness. This magnitude corresponds to a S/N of about 20.

Using the luminosity parameters for M33 derived by Baggett et al. (1998) by means of bulge-disc decomposition of its brightness profile, we expect that the total luminosity  $L_{B\odot}$  of the region of M33 used to build our PNLF comes from the disc. From that, adopting the specific planetary luminosity density for M31 (Ciardullo et al. 1989), we estimate a total of about 180 objects within 2.3 mag from the PNLF cutoff of about 20.3 mag. This figure has to be compared with the 75 candidate PNe that we effectively detected in M33 within the adopted completeness limit.

We applied the Eddington formula (Eddington 1913) to our data in order to correct for the effects of observational errors, and fit the resulting luminosity function for the complete sample of 75 PNe to the "universal" PNLF

$$N(m) \propto e^{0.307(m)} (1 - e^{3(m_* - m)}). \quad (2)$$

In Eq. (2)  $m$  is the observed  $[\text{O III}]$  magnitude from Eq. (1), and  $m_*$  is the apparent magnitude of the PNLF cutoff of M31 (Jacoby 1989).

This sample of 75 objects contains all candidate PNe within the established completeness limits regardless of their  $R$  ratio, since we already noticed that a substantial number of PNe are observed in the Galaxy with  $R < 1$ . Their luminosity function is

**Table 3.** Emission lines and continuum objects found in M33.  $H\alpha+[N\ II]$  and  $[O\ III]$  fluxes are in units of  $10^{-15}$  erg cm $^{-2}$  s $^{-1}$ . The last column gives the fluxes measured in the scaled Strömgen  $Y$  image, relative to the  $[O\ III]$  ones (see text).

id	R.A.	Dec	$F_{[H\alpha]}$	$F_{[O\ III]}$	$\frac{F_{[cont]}}{F_{[O\ III]}}$
1	1 31 56.3	30 28 23	0.0	0.9	2.7
2	1 32 09.3	30 26 02	4.2	3.7	5.8
3	1 32 16.0	30 09 14	20.8	8.1	7.0
4	1 32 21.6	30 21 16	62.2	23.6	8.5
5	1 32 26.6	30 24 05	6.2	1.3	1.9
6	1 32 27.0	30 25 29	56.6	19.1	0.5
7	1 32 28.5	30 28 16	2.0	3.0	1.9
8	1 32 33.9	30 22 35	6.0	1.0	0.9
9	1 32 36.8	30 20 19	24.3	17.1	4.9
10	1 32 42.4	30 25 22	2.0	0.3	6.4
11	1 32 43.8	30 13 26	6.7	0.7	22.
12	1 32 49.7	30 45 53	8.7	0.6	3.1
13	1 32 52.4	30 50 15	17.9	4.1	0.5
14	1 32 55.3	30 37 26	3.0	0.0	0.0
15	1 32 58.2	30 36 40	11.9	1.0	3.1
16	1 33 01.2	30 30 12	1.1	3.1	2.2
17	1 33 02.8	30 33 11	6.2	1.5	2.3
18	1 33 06.8	30 35 08	4.2	0.1	9.6
19	1 33 08.6	30 42 14	13.6	3.5	0.1
20	1 33 08.7	30 56 40	8.4	1.2	1.2
21	1 33 09.0	30 30 04	13.3	3.6	2.5
22	1 33 10.3	30 55 10	3.7	0.5	1.0
23	1 33 10.7	30 31 02	81.3	36.5	0.3
24	1 33 11.4	30 18 18	2.8	1.9	0.8
25	1 33 14.0	30 39 24	50.2	7.4	0.1
26	1 33 14.6	30 39 48	8.0	0.2	13.
27	1 33 15.0	30 51 21	4.4	0.1	22.
28	1 33 17.1	30 35 01	1.6	0.0	0.0
29	1 33 22.8	30 23 41	3.7	0.5	1.4
30	1 33 24.1	30 29 02	3.5	1.1	4.4
31	1 33 24.4	30 49 38	4.2	0.3	1.2
32	1 33 24.4	30 23 30	17.5	1.6	2.4
33	1 33 27.5	30 35 47	1.5	1.8	1.2
34	1 33 33.6	31 01 41	3.4	0.3	3.7
35	1 33 35.5	30 25 57	89.0	14.7	0.4
36	1 33 36.4	30 31 24	13.7	0.6	6.3
37	1 33 38.2	30 23 58	9.6	0.4	1.9
38	1 33 45.0	30 27 40	0.8	2.2	1.8
39	1 33 45.1	30 48 31	39.6	3.8	1.2
40	1 33 49.2	30 58 33	2.1	1.1	3.3
41	1 33 54.3	30 57 30	2.3	0.3	1.2
42	1 33 55.6	30 56 42	0.7	0.0	0.0
43	1 33 58.4	30 32 39	8.6	1.4	4.4
44	1 33 58.8	30 47 44	10.3	0.8	1.5
45	1 34 05.2	30 59 41	14.5	1.1	1.7
46	1 34 13.1	30 19 25	4.8	0.6	3.2
47	1 34 17.9	30 52 43	11.9	7.1	0.2
48	1 34 18.2	30 22 01	5.9	1.7	2.2
49	1 34 24.8	30 52 37	0.7	3.2	0.3
50	1 34 26.3	30 34 22	13.6	0.7	8.2
51	1 34 29.3	30 59 07	2.3	0.2	2.7
52	1 34 29.3	30 59 15	7.1	0.1	10.
53	1 34 30.9	30 49 36	4.6	0.2	1.2

**Table 3.** (continued)

id	R.A.	Dec	$F_{[H\alpha]}$	$F_{[O\ III]}$	$\frac{F_{[cont]}}{F_{[O\ III]}}$
54	1 34 31.8	30 21 09	10.0	1.0	5.9
55	1 34 36.6	31 02 39	7.4	0.4	2.9
56	1 34 39.2	30 46 52	3.4	0.0	0.0
57	1 34 40.0	30 47 52	3.4	0.8	1.8
58	1 34 41.9	30 56 02	17.1	3.6	0.8
59	1 34 42.5	30 55 41	26.3	3.6	0.3
60	1 34 46.5	31 08 37	3.3	0.2	1.7
61	1 34 49.8	30 47 29	2.4	0.0	0.0
62	1 34 51.1	30 37 44	47.4	19.8	0.3
63	1 35 32.6	30 47 02	3.4	0.0	0.0

presented in the upper panel of Fig. 4. In order to check whether exclusion of the objects with large  $H\alpha+[N\ II]$  over  $[O\ III]$  fluxes produces some effects on the PNLf, we also fit the theoretical formula to objects with  $R > 1$  only (Fig. 4, lower panel). Although the amplitude of the PNLf changes somewhat, in both cases we found the same apparent distance modulus of 24.62. This is because the most luminous objects in  $[O\ III]$  have generally also large  $R$  values (apart from few, but noteworthy exceptions). In fact, 80% of the candidates in the complete sample have  $R > 1$ , and if we restrict to the most critical luminosity range of the PNLf of M33, i.e. to magnitudes smaller than 21.6, 90% of the objects have  $R > 1$  and some 80% have  $R > 1.5$ . Thus the shape of the high luminosity tail of PNLf is not changed significantly by excluding objects with low  $R$  values, as confirmed by a further test in which we obtain the same results as above by considering objects with  $R > 1.5$  only.

The apparent distance modulus need to be corrected for foreground, Galactic reddening ( $E(B - V) = 0.045$ , Burstein & Heiles 1984) as well as for dust extinction within M33. The latter is an important source of uncertainty in the present analysis. Freedman et al. (1991) derived  $E(B - V) = 0.10 \pm 0.09$  (foreground + internal) for Cepheids in M33. Cepheids, however, are population I objects, and are located close or within the thin dust layer of M33. PNe are instead generally associated with an older disc population; in the Galaxy, for instance, they have a scale height above the disc two or three times larger than the dust layer (cf. Corradi & Schwarz 1995). Then some of our PNe will lie in front of the dust layer of M33 (which is seen relatively face-on), and will have a very small reddening; other objects will instead lie behind it, and will be characterized by a reddening similar (or only slightly larger) to that of the Cepheids. As a consequence, the average reddening for PNe is likely to fall between the foreground value ( $E(B - V) = 0.045$ ) and that of Cepheids ( $E(B - V) = 0.10$ ). The effect is difficult to quantify. As a test, we have computed the PNLf for PNe which are located at a galactocentric distance larger than one scale length of the exponential disc of M33 (530'', Baggett et al. 1998). Results obtained for other spiral galaxies (Xilouris et al. 1999) indicate that at such a distance the average, face-on extinction of a spiral galaxy is expected to be lower than 0.35 mag in  $V$ , corresponding to  $E(B - V) = 0.01$ . In addition, most of the selected PNe

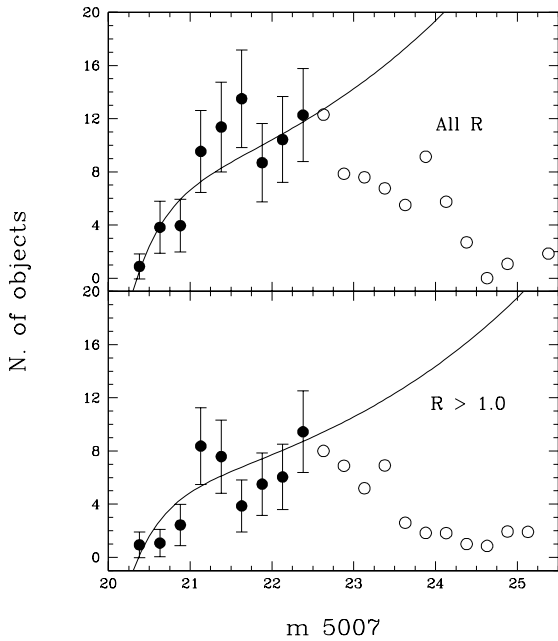


**Fig. 4.** The PNLF for M33, for all objects (upper box) and for those with  $R = \frac{[\text{O III}]}{H\alpha + [\text{N II}]} > 1$  (lower box). The adopted completeness limit is at 22.6 mag. Only the complete sample (full circles) is used to fit the theoretical PNLF (solid line).

are located in the inter-arm region, where extinction is expected to be even lower. By considering this subsample of PNe which is less affected by extinction within M33, we obtain the same apparent distance modulus as above, suggesting that our results are not strongly affected by dust internal to M33. Lacking of better estimates, we correct the apparent distance modulus using the value indicated by Freedman et al. (1991), and obtain a corrected modulus of  $24.62 \pm 0.25$ . The error is obtained by combining the error associated with our best least mean square fits ( $\pm 0.05$  mag) in quadrature with those associated with the photometric zero point (0.03 mag) and the adopted extinction (0.09 mag from Freedman et al. 1991). In addition, two systematic errors come from the uncertain definition of the empirical PNLF (0.05 mag) and the distance of the calibration galaxy M31 (0.10 mag).

All that finally leads to a distance to M33 of  $840 \pm 90$  kpc in excellent agreement with the value derived from the Cepheids method ( $840 \pm 20$  kpc, Freedman et al. 1991).

## 5. Summary and conclusions

We have detected 134 PN candidates in the spiral galaxy M33, by comparing [O III],  $H\alpha + [\text{N II}]$ , and continuum images taken with a panoramic mosaic detector attached to the 2.54 m INT. In addition, other 63 compact emission-line objects were identified which have a non-negligible continuum. Further spectroscopic studies are in order to determine their nature.

The PNe luminosity function of M33 is found to closely follow the general PNLF derived for other galaxies in the Local Group. From it, we derive a distance of M33 of  $840 \pm 90$  kpc, equal to the distance known from the Cepheids. This provides further support to the use of the PNLF as a valuable extragalactic distance indicator.

We plan to perform spectroscopic studies of the individual PNe candidates to fully verify their nature and derive information on their physical properties. This will also help in clarifying the possible misclassification of PNe with other emission-line objects in studies based on [O III],  $H\alpha + [\text{N II}]$  and continuum imagery only, a basic information when discussing the PNLF as an extragalactic distance candle.

*Acknowledgements.* We thank an anonymous referee for useful suggestions. The work of RLMC and AM has been supported by a grant of the Spanish DGES PB97-1435-C02-01.

## References

- Acker A., Ochsenbein F., Stenholm B., et al., 1992 *Strasbourg-ESO Catalogue Of Galactic Planetary Nebulae*
- Baggett W.E., Baggett S.M., Anderson K.S.J., 1998, ApJ 116, 1626
- Burstein D., Heiles C., 1984, ApJS 54, 33
- Ciardullo R., Jacoby G. H., Ford H.C., 1989, ApJ 334, 715
- Ciardullo R., Ford H.C., Neill J.D., Jacoby G.H., Shafter A.W., 1987, ApJ 318, 520
- Corradi R.L.M., Schwarz H.E., 1995, A&A 293, 871
- Corradi R.L.M., Villaver E., Mampaso A., Perinotto M., 1997, A&A 324, 276
- Dopita M.A., Hua C.T., 1997, ApJS 108, 105
- Eddington A.S., 1913, MNRAS 73, 359
- Freedman W.L., Wilson C.D., Madore B.F., 1991, ApJ 372, 455
- Jacoby G.H., 1989, ApJ 339, 39
- Jacoby G.H., 1997, in Planetary nebulae, IAU Symp. N. 180, H.J. Habing and H.J.G.L.M. Lamers eds, Dordrecht, Kluwer, p. 448
- Peimbert M., 1990, Rep. Prog. Phys. 53, 1559
- Xilouris E.M., Byun Y.I., Kylafis N.D., Paleologou E.V., Papamastorakis J., 1999, A&A 344, 868